

GT2011-45) *

ROTOR DYNAMIC FORCE COEFFICIENTS FOR THREE TYPES OF ANNULAR GAS SEALS WITH INLET PRESWIRL AND HIGH DIFFERENTIAL PRESSURE RATIO

Bugra H. Ertas*

Vibration/Dynamics Lab
Rotating Equipment Group
GE Research Center
Niskayuna, NY USA

Adolfo Delgado

Vibration/Dynamics Lab
Rotating Equipment Group
GE Research Center
Niskayuna, NY USA

Giuseppe Vannini

Conceptual Design
Advanced Technology
GE Oil and Gas
Florence, Italy

ABSTRACT

The following paper presents and compares rotordynamic force coefficients for three types of non-contact annular gas seals, which include a labyrinth (LABY), honeycomb (HC), and a fully partitioned damper seal (FPDS). These three annular seals represent the typical seal types used in process gas centrifugal compressors at the balance piston location or center seal location to limit internal leakage and ensure a robust rotordynamic design.

Tests were conducted on 170.6mm (6.716 in) diameter seals for rotor speeds up to 15krpm, inlet air pressure of 6.9 bar (100 psi), ambient back pressure, and with inlet gas preswirl. The three seals were designed to have the same nominal clearance and similar axial lengths. Testing was conducted on a controlled motion test rig possessing non-synchronous excitation capability up to 250Hz. Three different test methods were employed to give confidence in the rotordynamic coefficients, which include static force deflection tests, mechanical impedance tests, and dynamic cavity pressure tests. Results from experiments compare force coefficients for all seal configurations while paying special attention to the cross-over frequencies of the effective damping term. All seals possessed negative effective damping at lower excitation frequencies with inlet preswirl, where the straight-through FPDS possessed the lowest cross over frequency of 40Hz at 15krpm. The testing also revealed that the preswirl parameter had significantly more influence on effective damping levels and cross-over frequencies when compared to rotor speed.

INTRODUCTION

The balance piston seal or center seal in centrifugal compressors (Fig. 1) sustains the largest pressure drop in the machine and therefore plays an important role in successful full load operation at high rotor speeds. This is especially true for machines that generate higher discharge pressures, as the forces generated by the balance piston and center seals are directly

proportional to the fluid density in addition to the pressure differential across the seal [1]. For these high pressure and high-speed applications, damper seals often replace traditional labyrinth (LABY) seals so that stable and reliable rotordynamic operation is achieved. The two main types of gas damper seals used in industry are “textured” and “pocket” type annular seals. One of the seals evaluated in this work is the honeycomb (HC) seal. The HC seal is a type of textured damper seal that has been used to solve dynamic stability problems in centrifugal compressors [2]. These seals possess high direct damping and positive stiffness; however also generate destabilizing stiffness cross coupling [3].

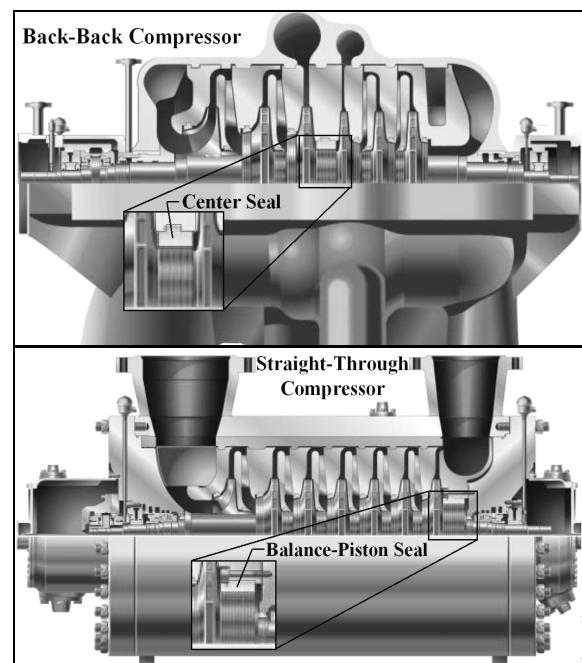


Figure 1. Seals in centrifugal compressors

* Mechanical Engineer, Phone: (518) 387-7466, Fax: (518) 387-5459, Email: ertas@research.ge.com.

Ultimately, the balance between direct damping and cross-coupled stiffness determine the effective damping [4] of the seal, which represents the net damping capability. Past experiments on HC seals with inlet preswirl conditions and/or rotor speed [3,5] show that the effective damping is negative for lower frequency ranges and transitions to a positive effective damping value as excitation frequency increases. The transition point from negative effective damping to positive effective damping, or crossover frequency, is used as a critical metric in engineering the location of the first fundamental subsynchronous forward whirl rotor mode. Rotor modes residing below the crossover frequency are at risk of rotordynamic subsynchronous instabilities that can prevent the full operational capability of the machine. Ongoing research [6,7] is striving to lower the effective damping crossover frequency in efforts to maximize the useful operating frequency range.

The other types of damper seals used in industry [8] are “pocket” type annular gas seals, as shown in Fig. 2. These types of seals are constructed by inserting or machining baffle walls between paired blades creating circumferential pockets or cavities. The pocket damper seal (PDS) was developed [9] partly by leveraging concepts first introduced by Alford [10] on forces generated in labyrinth seals. Alford’s work showed that diverging clearance labyrinths created positive direct damping and negative stiffness while converging clearance labyrinths produce a negative damping and a positive stiffness. Therefore, PDS were developed with diverging clearances so that high direct damping was generated, while also consequently possessing an appreciable negative direct stiffness. The diverging clearance is created for each cavity by machining a downstream notch for paired blades. The rows of cavities, for the PDS, are then separated by plenums containing no baffle walls. This is a key design feature of a PDS, because the function of the plenums is to maintain constant boundary pressures for the cavities during rotor whirl, as Alford’s analysis assumed constant boundary pressure on each side of a two blade labyrinth seal. Following the development of the PDS, a FPDS was tested on a rotating rig [11]. A FPDS as shown in Fig. 2, uses baffle walls throughout the entire axial length of the seal and contains no plenums. Fully partitioning the seal by using an axially uninterrupted baffle wall creates alternating diverging and converging cavities. Even though the test seal possessed converging cavities, the critical speed transition tests [11] using rotor imbalance as the excitation to the rotor bearing system revealed a seal with high damping and positive stiffness. Further testing on a component level controlled motion test rig [12] of the FPDS confirmed the previous critical speed results [11] by measuring high direct damping compared to the PDS and also direct positive stiffness. Dynamic pressure measurements in the seal cavities at 0rpm with no preswirl revealed that the higher direct damping in the FPDS was generated through the contribution of positive direct damping from the converging clearance cavities, which are the smaller cavities with shorter axial pitch shown in Fig. 2. Although having converging clearance geometries, the smaller cavities did not behave as Alford predicted due to the boundary pressure being time dependent and not constant with rotor vibration. Additionally, unlike the conventional PDS, the FPDS revealed a small negative direct stiffness coefficient at lower frequencies that transitioned to positive stiffness as excitation frequency was increased. The dynamic pressure testing [12] also revealed same-

sign cross-coupled stiffness at 0rpm and no preswirl. The past testing on FPDS [11,12] was with seal design having notches as shown in Fig. 2. These past tests on notched FPDS were conducted with no inlet preswirl.

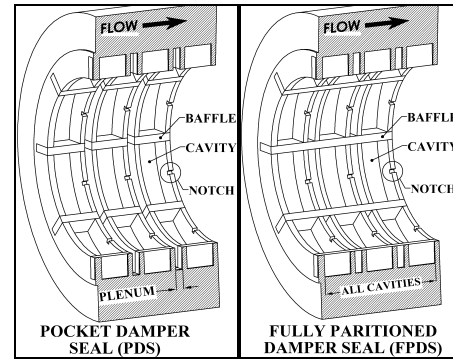


Figure 2. PDS vs. FPDS

As early as 1980, Benckert and Wachter [13] conducted tests on what can be considered as a pocket style gas seal. Although not referred to as a damper seal, one of the configurations included “swirl-webs” (analogous to baffles) between 17 labyrinth seal blades (Figure 3) creating 16 rows of 4 circumferential pockets. This test labyrinth seal with swirl webs without notches (Figure 3) is the simplest embodiment of a pocket style annular gas seal, essentially categorized as a “straight-through” FPDS. The experiments included several static force-deflection rotating tests in efforts to extract zero frequency stiffness coefficients. Benckert and Wachter’s testing did employ preswirl in experiments, but lacked the capability to perform dynamic testing. This limitation prevented the measurement of direct damping, which is a key term in calculating the effective damping of a seal. Their results showed that inserting swirl webs into the 17 blade labyrinth seal significantly increased the destabilizing static cross-coupled stiffness coefficient.

Although extensive testing has been performed on these three types of pocket style annular gas seals, measurements of effective damping and crossover frequencies with inlet preswirl are not available, preventing direct comparison with HC and LABY seals under inlet preswirl conditions.

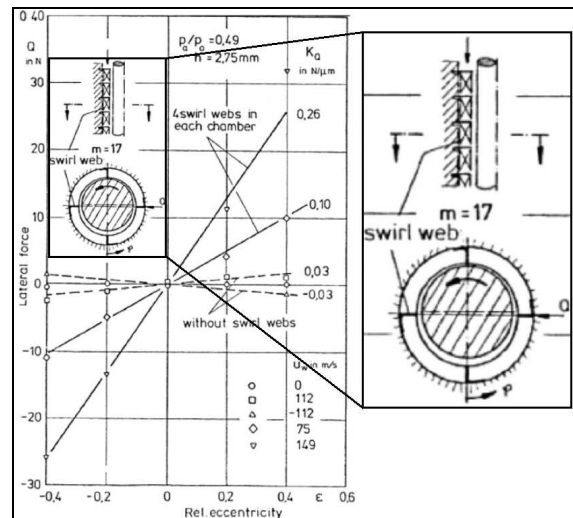


Figure 3. Benckert and Wachter’s testing [13]

The main objective of this work was to measure the rotordynamic stiffness and damping coefficients of a FPDS without notches (straight-through), while subjecting the seal to inlet preswirl and rotor speed. The results focus on comparing force coefficients and crossover frequencies to typical labyrinth and honeycomb seal designs.

TEST SEALS

The test seal designs are shown in Fig. 4 and described in Table 1. The 14 blade LABY seal and HC seal were representative of best practice standards for centrifugal compressor balance pistons. The FPDS was designed with the same clearance however has a larger L/D. All seals were tested with 6.9 bar preswirl plenum pressure, 50-60F inlet temperature, and 1 bar (atmosphere) backpressure for zero velocity inlet preswirl and also inlet preswirl flow velocity of 60m/s. The test

speeds chosen for comparison are 7krpm and 15krpm on a 170mm diameter rotor. The FPDS has 8 blades making 7 axial rows of 8 circumferential cavities, where cavity 1 is the most upstream cavity. Two cavity depths are tested for the FPDS.

Table 1. Test seal parameters

PARAMETER	LABY	HC	FPDS1	FPDS2
Seal Length (mm)	65	65	102	102
Rotor Diameter (mm)	170	170	170	170
Seal L/D	0.38	0.38	0.60	0.60
Radial Clearance (mm)	0.30	0.30	0.30	0.30
Number of Blades	14	N/A	8	8
Cavity/Cell Depth (mm)	4	2.6	3.175	6.35
Projected Area On Rotor (mm ²)	11050	11050	17340	17340
Projected Area Factor	1.6	1.6	1	1
Preswirl Velocity (m/s)	60	60	60	60

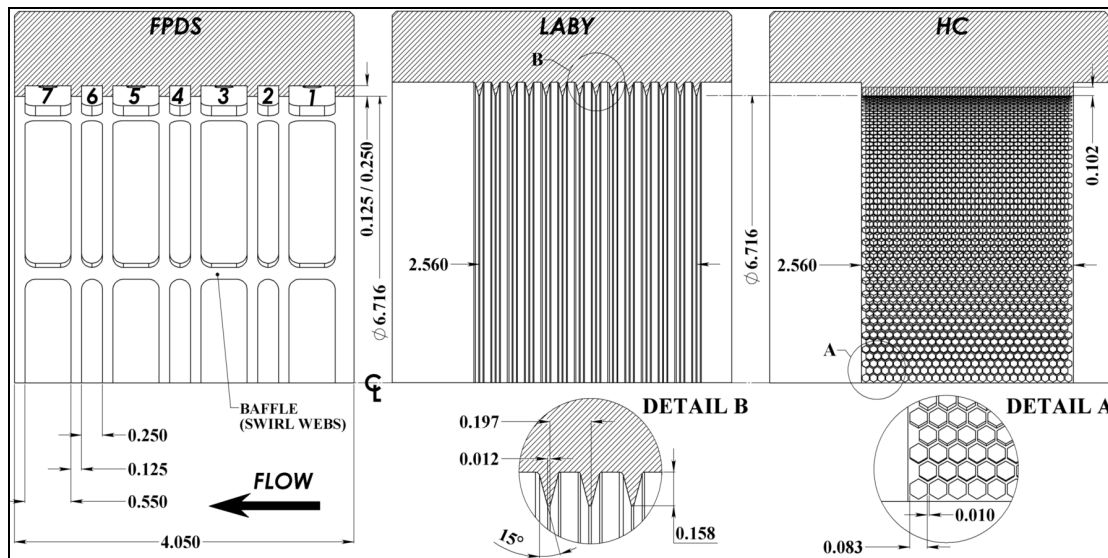


Figure 4. Test seal geometry (dimensions in inches)

EXPERIMENTAL METHODS AND TEST SETUP

The test facility used to evaluate the test seals is a controlled motion component level rotating test rig. The basic testing scheme and layout draws from past work conducted by Childs and Hale [14]. The experimental set-up is shown in Figs. 5-7. Figure 5 displays a cross-sectional view of the test rig. The general testing approach inputs controlled motion excitations through the test seal housing rather than relying on rotor imbalance for force input. Therefore, the seal housing is compliantly supported using six pitch stabilizers that interface the FWD and AFT bearing supports. The pitch stabilizers ensured parallelism between the stator housing central axis and the rotor spin axis, whereas the hydraulic shakers maintained concentricity between the two elements. The stator housing and rotor centering capability was $\pm 5\mu$. The precision balanced rotor system was straddle mounted using two sets of rigidly mounted angular contact ball bearings. This enabled the first critical speed to be located at 24krpm, well beyond the test frequency range of 250Hz and max rotor speed of 15krpm. The two test seals were assembled in a back-to-back configuration to cancel thrust and were axially constrained using 8 through-bolts. Flow enters the system at the stator midplane into the inlet plenum. Then the flow passes through a preswirl ring (Fig. 5 and

7) and enters the preswirl plenum with positive (in direction of rotor rotation) tangential flow velocity. Flow is then directed through the test seal and discharges to ambient pressure conditions. End seals outboard of the test seals were not used in this set up. This prevented the control of back-pressure in the system, however contributed to a more accurate and straightforward baseline measurement.

Several static and dynamic measurements were taken during the testing. Static measurements that defined the test conditions included inlet temperature, inlet plenum static pressure, preswirl plenum static pressure, and rotor speed. Also, 2-hole pitot tubes were used in the preswirl plenum to capture the tangential flow velocity of the gas before entering the test seals, which varied $\pm 5\%$. Dynamic measurements both in X and Y directions included force, relative motion of the stator and rotor, and stator housing acceleration. Dynamic cavity pressures were also measured for the FPDS for cavities labeled from 1-7.

Three different experimental techniques were used to extract force coefficients: 1) static force-deflection tests, 2) mechanical impedance tests, and 3) dynamic cavity pressure tests. The seal forces can be modeled using Eq. 1, which relates the forces due to rotor motion and velocity through direct (K_{xx} , K_{yy} , C_{xx} , C_{yy}) and cross-coupled (K_{xy} , K_{yx} , C_{xy} , C_{yx}) linear force coefficients.

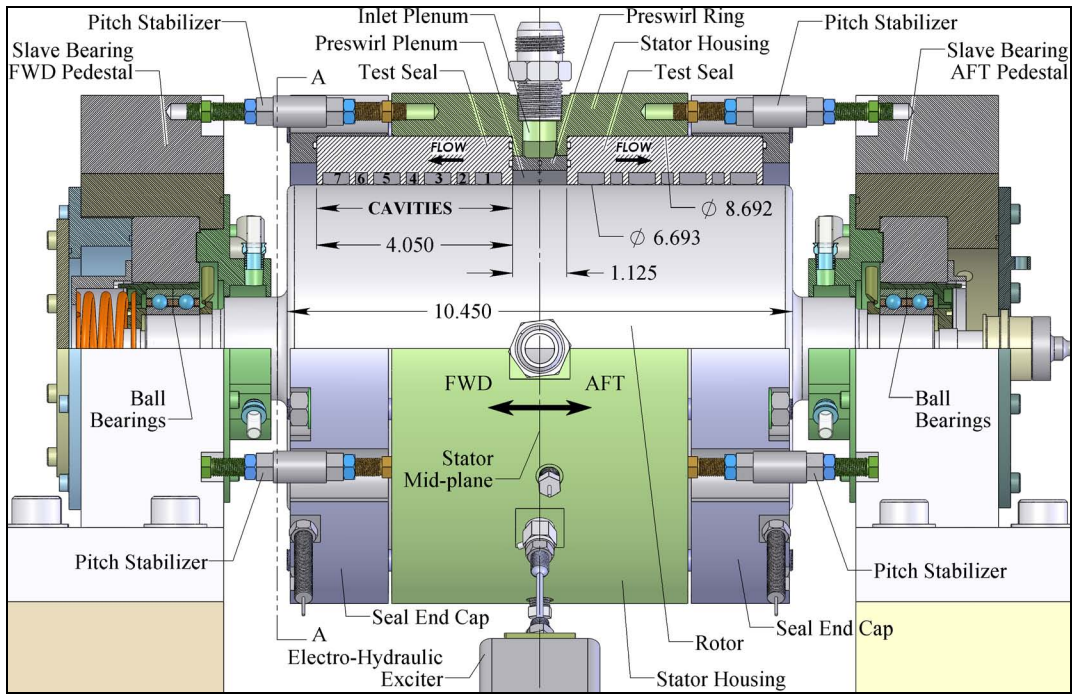


Figure 5. Test rig cross section (dimensions in inches)

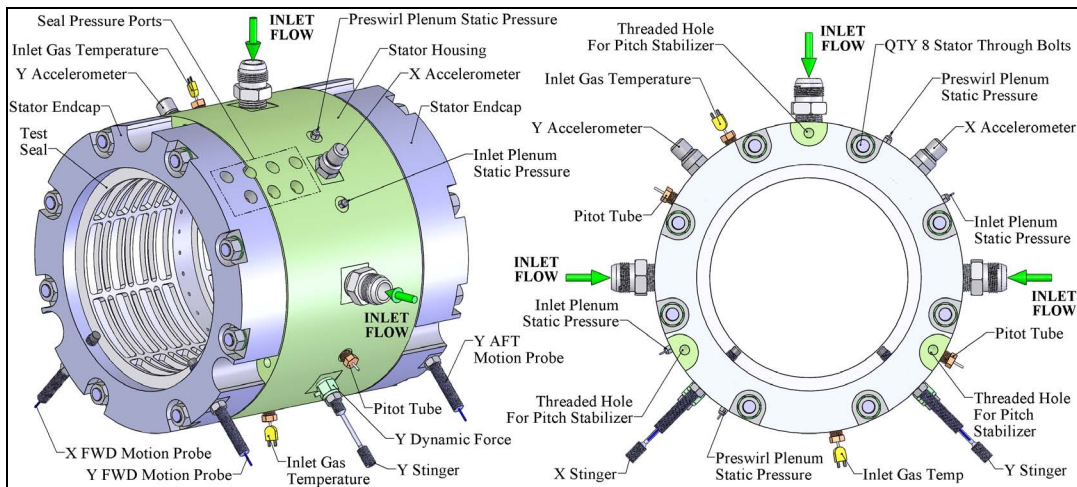


Figure 6. Stator and seal housing assembly

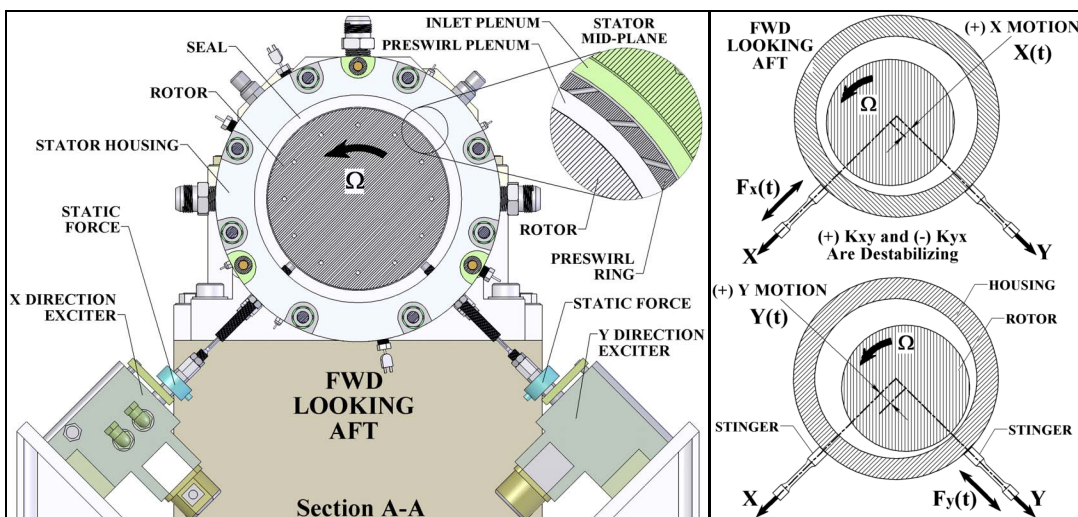


Figure 7. Inlet preswirl and coordinate system convention

Test methods 1 and 2 use the same reduction methods and equations, which are based on techniques advanced by Rouvas and Childs [15]. Neglecting added mass terms from the seals and considering small perturbations about the equilibrium position, Equation 1 is transformed to the frequency domain (Eq. 2) using a Fourier transform.

$$-\begin{bmatrix} F_X \\ F_Y \end{bmatrix} = \begin{bmatrix} K_{XX} & K_{XY} \\ K_{YX} & K_{YY} \end{bmatrix} \cdot \begin{bmatrix} X \\ Y \end{bmatrix} + \begin{bmatrix} C_{XX} & C_{XY} \\ C_{YX} & C_{YY} \end{bmatrix} \cdot \begin{bmatrix} \dot{X} \\ \dot{Y} \end{bmatrix} \quad (1)$$

Two independent excitations in the X and then Y directions are imposed on the system to yield 4 independent equations (Eq. 3), where D_{ij} is the relative displacement of the stator housing respect to the rotor, A_{ij} is the stator acceleration, and m is the stator mass. The first subscripts in Eq. 3 represent the direction of the excitation or test.

$$\begin{bmatrix} F_X \\ F_Y \end{bmatrix} = \begin{bmatrix} H_{XX} & H_{XY} \\ H_{YX} & H_{YY} \end{bmatrix} \cdot \begin{bmatrix} D_X \\ D_Y \end{bmatrix} ; H_{ij} = K_{ij} + i(\omega \cdot C_{ij}) \quad (2)$$

$$\begin{bmatrix} F_{XX} - m \cdot A_{XX} & F_{YX} - m \cdot A_{YX} \\ F_{XY} - m \cdot A_{XY} & F_{YY} - m \cdot A_{YY} \end{bmatrix} = \begin{bmatrix} H_{XX} & H_{XY} \\ H_{YX} & H_{YY} \end{bmatrix} \cdot \begin{bmatrix} D_{XX} & D_{YX} \\ D_{XY} & D_{YY} \end{bmatrix} \quad (3)$$

An example static force deflection test is shown in Fig. 8. These static tests were performed to support the findings from the mechanical impedance tests (second method). In particular, the signs of the stiffness cross-coupling terms were of importance. Figure 8 illustrates two different tests displayed in two plot formats. The top plots show the static displacement of the seal housing as a function of the force input. Static forces were applied to the system through two orthogonally mounted electro-hydraulic shakers (Fig. 7) used in force control. Tests were conducted by inputting a known force in a single direction while monitoring the displacement of the stator housing. Both an unpressurized 0rpm baseline test and pressurized test are shown. The bottom plots of Fig. 8 display the actual housing movement of the rotor spin axis with respect to the stator housing (units in mils) for the two tests. As expected, the baseline shows very little cross coupling whereas the pressurized test with preswirl shows significant destabilizing cross-coupled stiffness. Using these two sets of data the static (zero frequency) stiffness matrix of the seals were calculated.

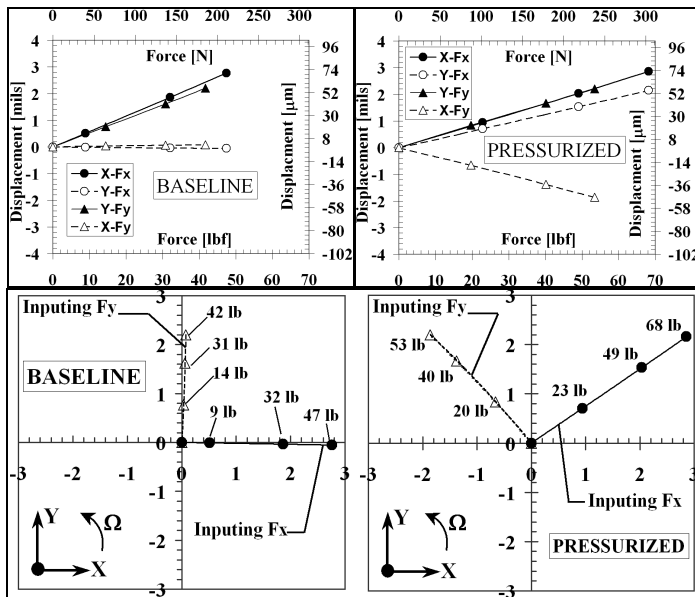


Figure 8. Example static force-deflection tests

The second method used in this work is the mechanical impedance method that requires the measurement of external dynamic forces imposed on the stator housing in combination with relative stator motion and stator acceleration. The testing scheme employed two independent dynamic excitations in the X and Y directions comprising a pre-engineered multitone waveform including frequencies between 20Hz and 250 Hz. Thirty consecutive averages were taken and processed using cross-spectral density analysis to reduce noise in the test, as presented in [15]. An example X direction excitation is shown in Fig. 9. Both the X and Y direction time varying force and motion are shown along with their representative Fourier transforms. The peak spectral vibration (displacement) amplitude for each frequency component was targeted to be 0.1mil (2.5 μ) by optimizing the pseudorandom force waveform. The calculation of the full set of frequency dependent system impedances (H_{ij}) also required a test in the Y direction as well as baseline tests. The baseline test was performed prior to pressurizing the seals at 0rpm, followed by a pressurized test at the specified operating conditions. The subtraction of the baseline impedances from the test impedances yielded the seal impedance (Eq. 4).

$$\begin{bmatrix} H_{XX} & H_{XY} \\ H_{YX} & H_{YY} \end{bmatrix}_{SEAL} = \begin{bmatrix} H_{XX} & H_{XY} \\ H_{YX} & H_{YY} \end{bmatrix}_{TS} - \begin{bmatrix} H_{XX} & H_{XY} \\ H_{YX} & H_{YY} \end{bmatrix}_{BL} \quad (4)$$

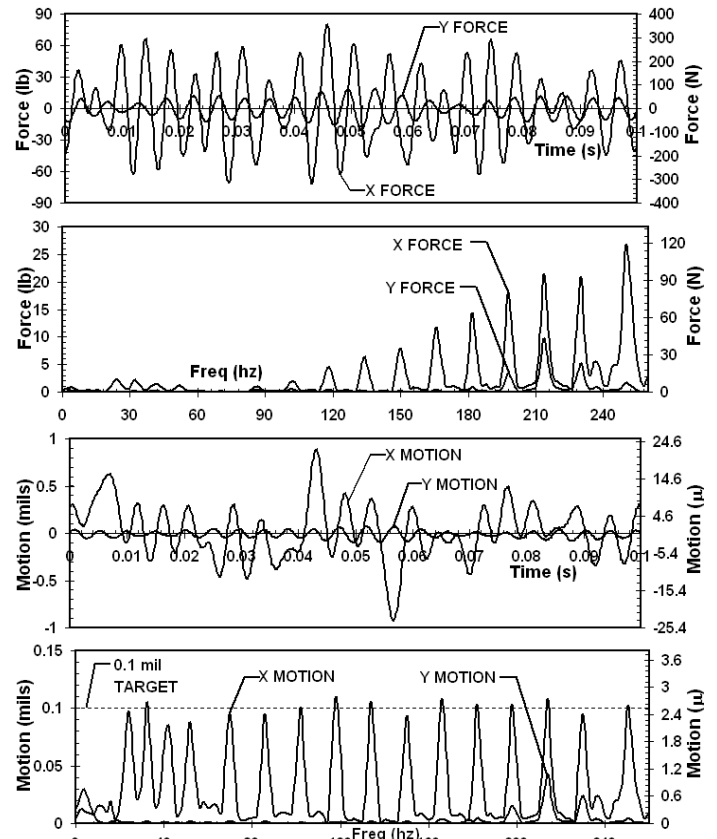


Figure 9. X excitation: Mechanical impedance method

The third method used to extract force coefficients and crossover frequencies for the FPDS is the dynamic pressure method [12,16]. This method does not require a baseline measurement because the seal forces are directly measured through dynamic pressure transducers in the seal cavities. Figure 6 shows the pressure ports for the pressure transducers, which

are installed in a single axial row of cavities that are aligned with the X direction. The designation for the cavity numbers is shown in Figs. 4 and 5. Figure 10 shows an example of the 7 axial cavities dynamic pressures due to an X direction motion of the stator housing assembly. These pressures are integrated over the projected area of the cavity (Eq. 5) and are transformed to cavity forces as a response to stator motion. Using the Fourier transform, frequency domain reduction of the force coefficients was performed following the relationship shown in Eq. 6, where φ_{ij} is the pressure impedance of the seal. Linear single frequency excitations were performed in several directions using simultaneous X and Y shaker motions to calculate the total seal impedance from a single axial row of cavity pressure measurements. All cavity coefficients thereafter are assembled to yield the overall seal coefficients contributed from 56 cavities.

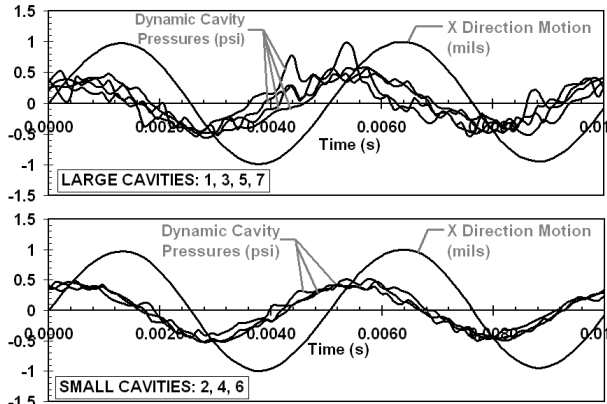


Figure 10. X excitation: Pressure method 198hz FPDS2

$$\bar{F}_X = \sum_{k=1}^{56} \left[\int_A (P^k \cdot \cos \theta_0) dA \right], \bar{F}_Y = \sum_{k=1}^{56} \left[\int_A (P^k \cdot \sin \theta_0) dA \right] \quad (5)$$

$$\begin{bmatrix} \bar{F}_{XX} & \bar{F}_{YX} \\ \bar{F}_{XY} & \bar{F}_{YY} \end{bmatrix} = \begin{bmatrix} (\phi_{XX}) & (\phi_{XY}) \\ (\phi_{YX}) & (\phi_{YY}) \end{bmatrix} \cdot \begin{bmatrix} D_{XX} & D_{YX} \\ D_{XY} & D_{YY} \end{bmatrix} \quad (6)$$

$$\varphi_{ij} = (K_{ij} + iC_{ij}\omega) \quad (7)$$

RESULTS AND DISCUSSION

This section presents the experimental results representative of single seal coefficients. All results correspond to tests at 6.9bar preswirl plenum pressure and atmospheric backpressure. Tests using preswirl, generated 60m/s tangential flow velocity in the preswirl plenum location.

The direct and cross-coupled stiffness results from the static force deflection testing are shown in Figs. 11-13. Figure 11 shows the test results with preswirl at 0rpm. Average direct stiffness coefficients for the FPDS are negative, whereas the LABY and HC seals show positive direct stiffness. All seals in Fig. 11 indicate destabilizing stiffness cross coupling (same magnitude opposite sign), which are larger in absolute magnitudes when compared to the direct stiffness values. The cross-coupled stiffness is smallest for the LABY seal under these conditions. Next, static testing was performed for a zero preswirl condition and focused on the influence of rotor speed Figs. 12-13. For direct stiffness, the rotating tests yield values that are comparable to the tests performed with preswirl at 0rpm. Interestingly enough, results show that rotor speed slightly increases the static direct stiffness of the FPDS and HC, whereas

the stiffness of the LABY seal slightly decreases with increasing rotor speed. Figure 13 presents the static cross-coupled stiffness coefficients with increasing rotor speed. Results show a linearly increasing destabilizing cross-coupled stiffness coefficient with rotor speed for the FPDS and HC seal. However, rotor speed has very little influence on the LABY seal cross-coupled stiffness. In fact, the cross-coupled stiffness of the LABY seal is almost too small to be measured when not subjected to preswirl. The results of the static force deflection tests confirm that the cross-coupled stiffness forces generated by preswirl and rotor speed create $(+)K_{xy} = (-)K_{yx}$ at 0Hz. Furthermore the results confirm Benckert and Wachter's [13] results showing higher cross-coupled stiffness for the seal with baffles compared to the labyrinth seal.

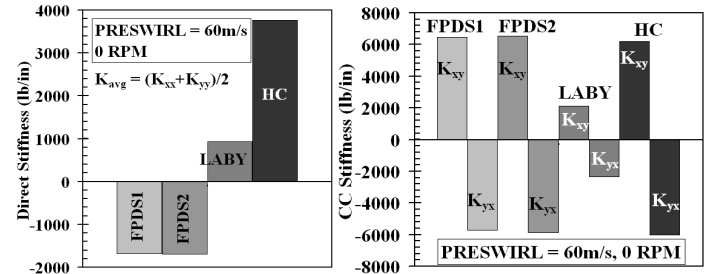


Figure 11. Static stiffness with preswirl and no rotation

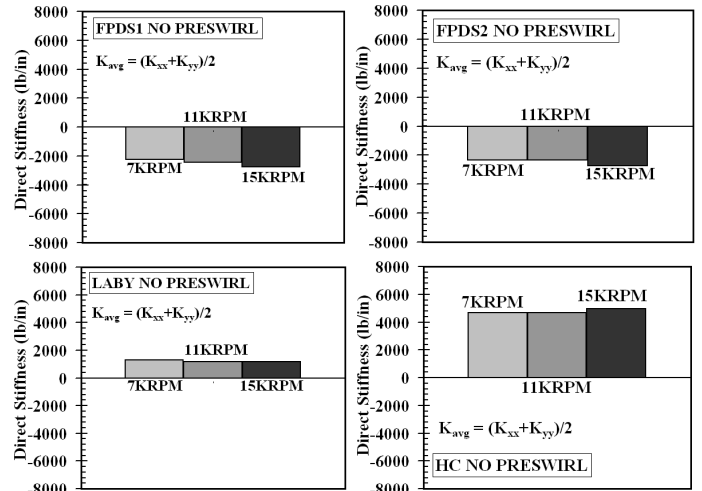


Figure 12. Direct static stiffness with no preswirl

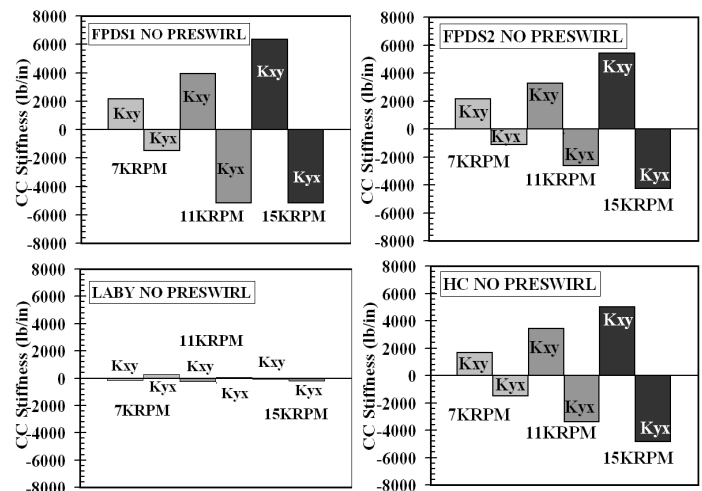


Figure 13. Cross-coupled static stiffness with no preswirl

Figures 14-16 present the results for the mechanical impedance testing. For brevity the X and Y direction coefficients are averaged and the cross-coupled damping term is not presented, as this term was calculated to be small and has no influence on the seal effective damping term. Additionally, only the FPDS1 configuration is compared to the LABY and HC seals. Error bars represent $\pm 2\sigma$ uncertainty.

Figure 14 shows the results for the direct stiffness and damping calculated using the mechanical impedance method. Each graph displays results with no preswirl (NPS) and with preswirl (PS) at 7krpm and 15krpm. The highest direct stiffness was measured using the HC seal for both speeds and preswirl values. The FPDS initially possesses small negative stiffness at low frequencies and then transitions to positive stiffness values at frequencies above 75Hz. The LABY seal shows small positive stiffness at low frequencies and then crosses over between 125-150 Hz to negative stiffness following a trend indicative of a parabolic decay. Preswirl has a stiffening effect for the HC seal and FPDS, but has a softening effect on the LABY seal. Increasing the rotor speed creates an appreciable increase in direct stiffness for the HC seal, however this is only observed for the case with PS. The direct damping results are shown in the bottom two plots in Fig. 14 and shows that the LABY seal possesses the lowest damping values that are relatively constant with excitation frequency. The frequency independent direct damping term is consistent with results presented for past labyrinth seal testing [17]. Unlike the direct damping behavior of the LABY seal, the FPDS and HC seal yield significantly higher values and show strong frequency dependence. The FPDS shows

higher damping values, but also has a larger projected area on the rotor. One notable difference between the FPDS and HC seal direct damping results was the influence of rotor speed on the coefficients. Increasing rotor speed for the FPDS results in a significant increase in the direct damping term ($\sim 20\%$ increase). On the other hand, the HC seal direct damping coefficient shows little dependency on rotor speed.

The next sets of results from the mechanical impedance testing are the cross-coupled stiffness and effective damping coefficients, shown in Figs. 15-16. For a system which exhibits $(+)K_{xy} = (-)K_{yx}$, the effective damping can be defined as [4]:

$$[C_{EFF}]_X = C_{XX} - \frac{K_{XY}}{\omega}, \quad [C_{EFF}]_Y = C_{YY} + \frac{K_{YX}}{\omega} \quad (8)$$

The LABY seal cross-coupled stiffness changes very little with rotor speed and for the cases with NPS the values are small. Additionally, the coefficients are frequency independent. Figure 15 shows that the LABY seal cross-coupled stiffness identified from the mechanical impedance and static tests (Fig.11) yield similar values ($\sim 2,000\text{lb/in}$), which corroborates the weak dependency of the cross-coupled coefficients on rotor speed and excitation frequency for this seal. The FPDS shows larger cross-coupled stiffness coefficients than the LABY, while having comparable values to the HC seal. For both the HC seal and FPDS increasing rotor speed from 7krpm to 15krpm for the NPS cases increases the lower frequency range cross-coupled stiffness values. The effect of preswirl is more prevalent for the lower rotor speed of 7krpm when compared to 15krpm.

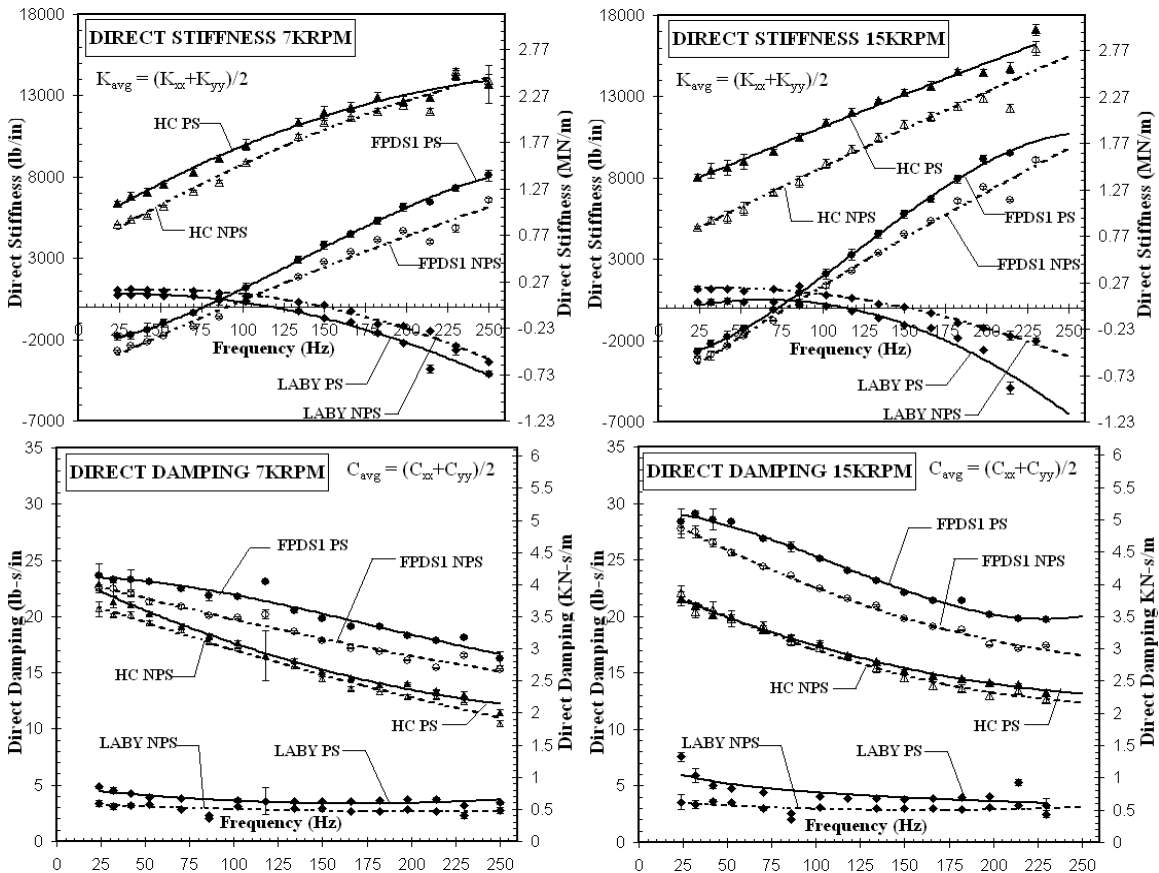


Figure 14. Direct Stiffness and Damping: 7krpm and 15krpm: mechanical impedance method

Figure 16 shows the final plot for the mechanical impedance test comparisons, which is the effective damping. All seals generate positive effective damping throughout the entire test frequency range for the 7krpm and NPS cases, where the HC and FPDS produce significantly more damping compared to the LABY. However, when preswirl was introduced the effective damping

values crossed over to negative values. The results show that FPDS and HC share very similar crossover frequencies of 50Hz whereas the LABY seal shows crossover at ~100Hz. The NPS cases for 15krpm are showing the FPDS and HC seal with crossover frequencies of ~30hz, whereas the LABY seal has purely positive damping throughout the test frequency range.

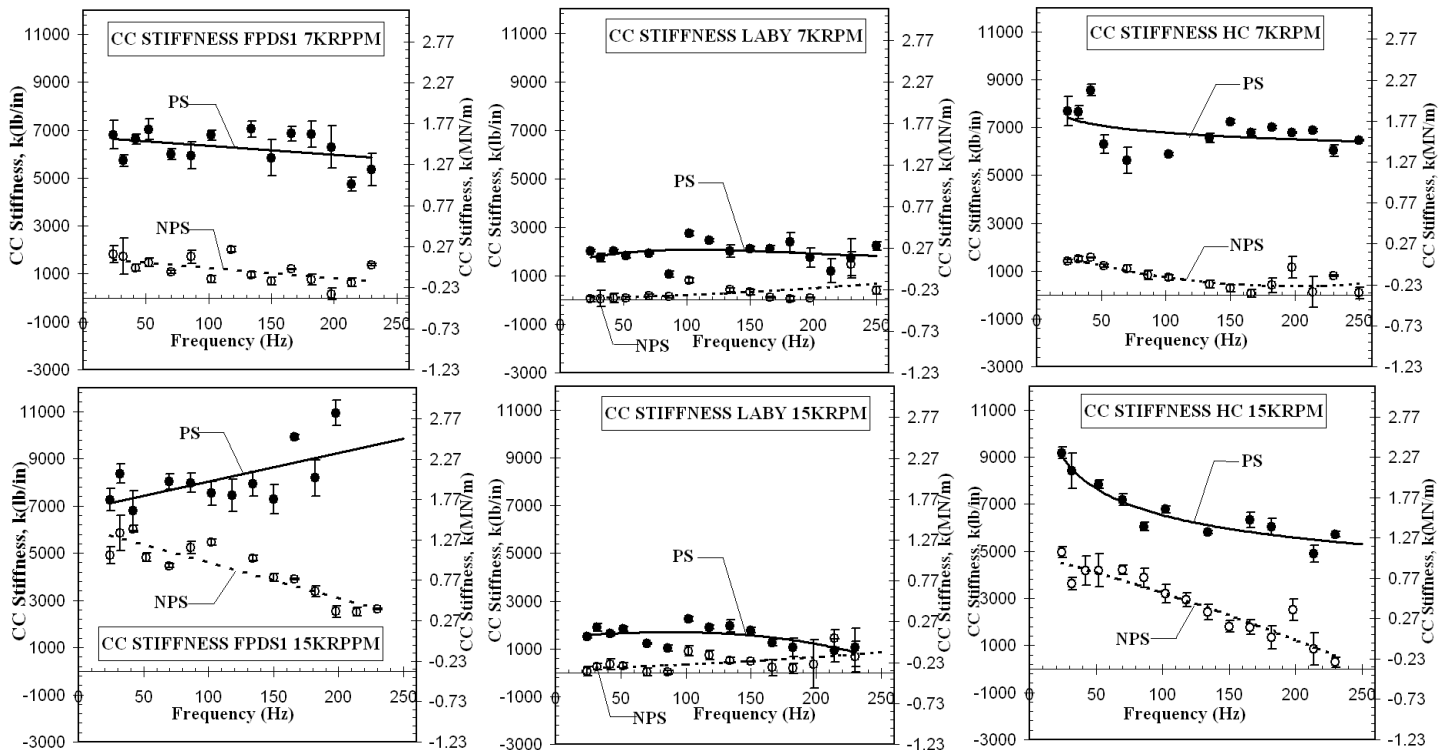


Figure 15. Cross-Coupled Stiffness 7krpm and 15krpm: mechanical impedance method

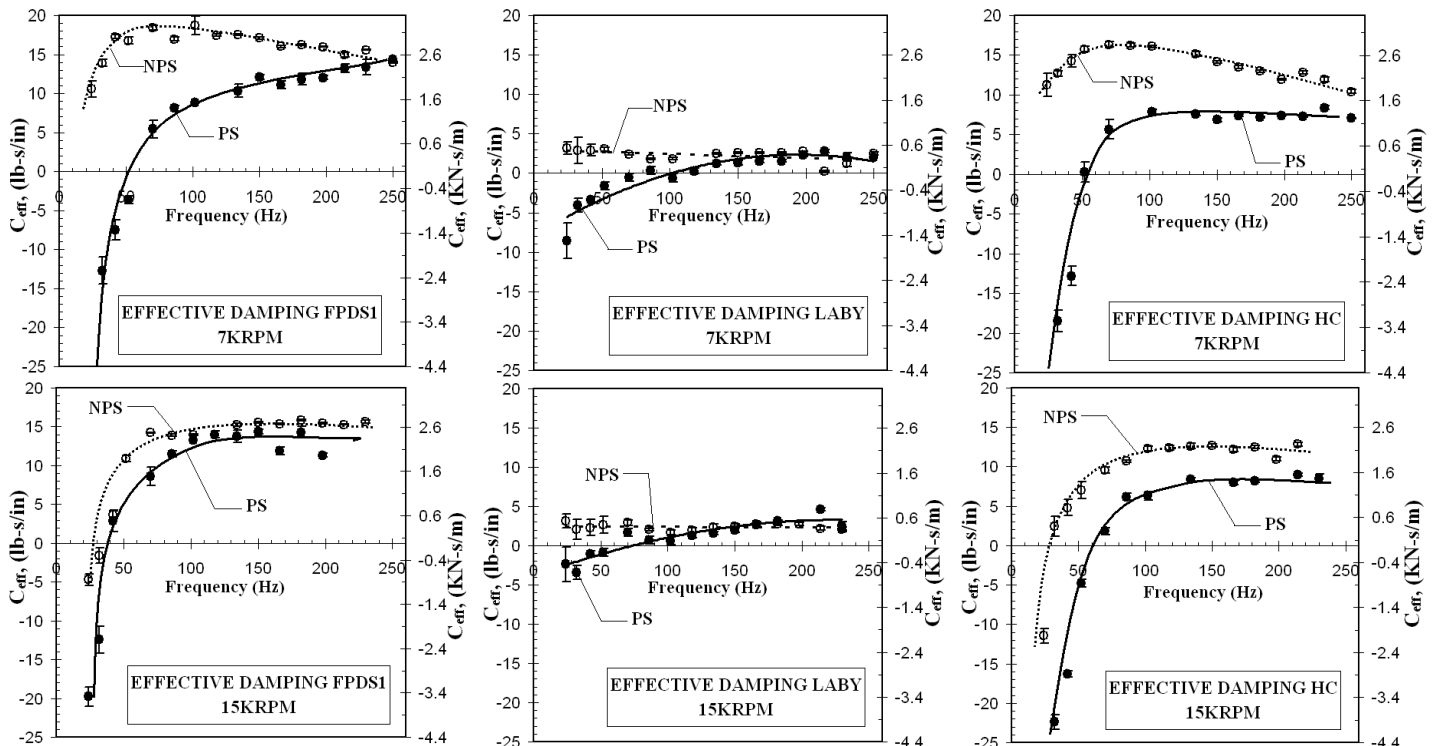


Figure 16. Effective damping 7krpm and 15krpm: mechanical impedance method

The final case in Fig. 16 is the 15krpm with PS. The crossover frequencies for the LABY seal and FPDS actually decrease when compared to the 7krpm case. This is attributed to the direct damping coefficient increasing with rotor speed while the influence of rotor speed on the cross coupling stiffness is small. Contrary to this behavior, the HC seal crossover frequency increases from 50Hz to 60Hz. This shift is due to a direct damping coefficient that was unchanged when increasing rotor speed from 7krpm to 15krpm in combination with a slight increase in cross-coupled stiffness for the 15krpm case. The HC seal crossover frequency range is consistent with existing test data. Figure 17 shows effective damping results from high inlet pressure tests (70bar) on HC seals [3] and presents two sets of data for different pressure ratios revealing similar crossover frequencies of ~65Hz. The close correlation between the current HC seal test case and the past higher pressure testing suggests that the cross-coupled stiffness forces and direct damping forces scale similarly with pressure and pressure ratio.

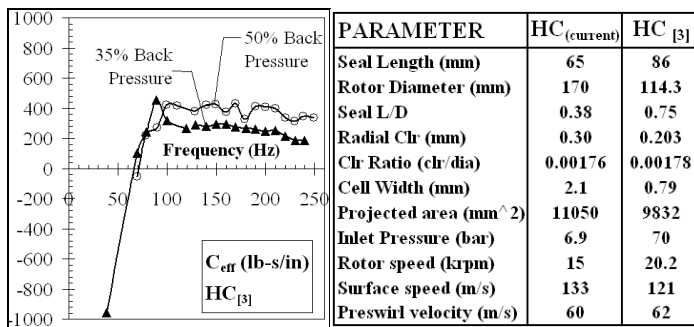


Figure 17. Effective damping results of HC seal tests from [3]

The next portion of the results focuses on dynamic pressure testing on the FPDS2. These tests served to gain further insight to the influence of rotor speed versus preswirl on seal stability and compare results to the mechanical impedance method. It is important to note that the pressures are integrated only over the cavity area. The close clearance flow regime under the blades was not accounted for due to the inability to measure pressure in this region.

The first set of plots (Fig. 18) shows the comparison of full seal coefficients between the mechanical impedance method and dynamic pressure method for 0rpm with PS and 15krpm with NPS. The trends of the direct stiffness and damping coefficients are identical for both methods, though the dynamic pressure method yields smaller valued coefficients. This can be attributed to not accounting for the blade areas and pressures as the area of this region is ~30% of the total seal area. The cross-coupled stiffness values present good agreement between the two methods in terms of their trend, however the dynamic pressure under-calculates the coefficients. Despite the discrepancies between both methods in terms of the direct damping and cross-coupled stiffness, the effective damping for both methods yields similar crossover frequencies. In terms of operation conditions, the results indicate that preswirl has a much stronger destabilizing effect when compared to rotor speed as shown in the difference between crossover frequencies of 25hz versus 50hz.

The next sets of plots (Fig. 19-20) are showing the decomposed cavity level force coefficients of the pressure results presented in Fig. 18.

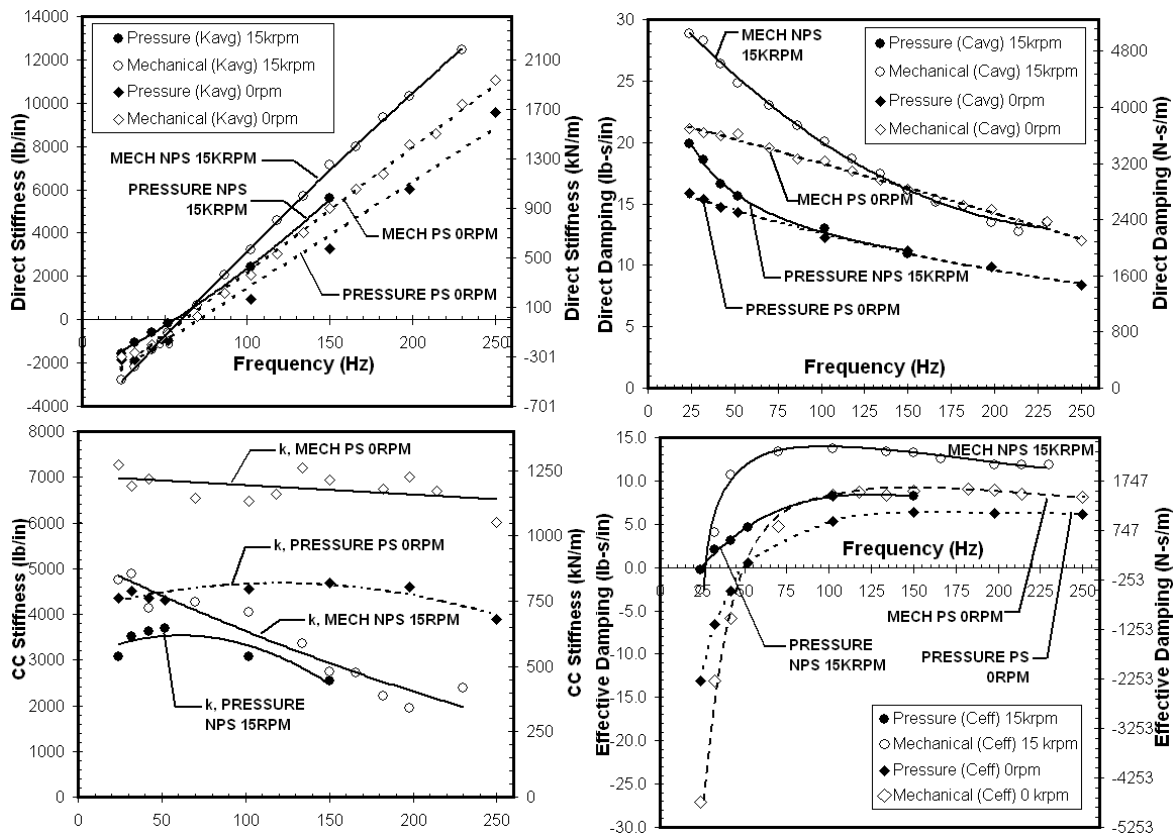


Figure 18. Rotordynamic coefficients: preswirl vs. rotor speed FPDS2

Only the cross-coupled stiffness and effective damping are presented, as crossover frequencies are the main focus. Figure 19 shows results for 0rpm and with PS, where the left side plots represent the large cavities 1, 3, 5, and 7 and the right side plots represent the smaller cavities 2, 4, and 6. The cross-coupled stiffness values are shown to be highest at the upstream location of the seal and decreases as the cavity number increases. The

effective damping presents an opposite trend, as the largest positive valued damping coefficients are generated at the down stream end of the seal, and the lowest valued effective damping is in the leading portion of the seal. Figure 20 represents the 15krpm with NPS case and shows a very different behavior when compared to the results in Fig. 19.

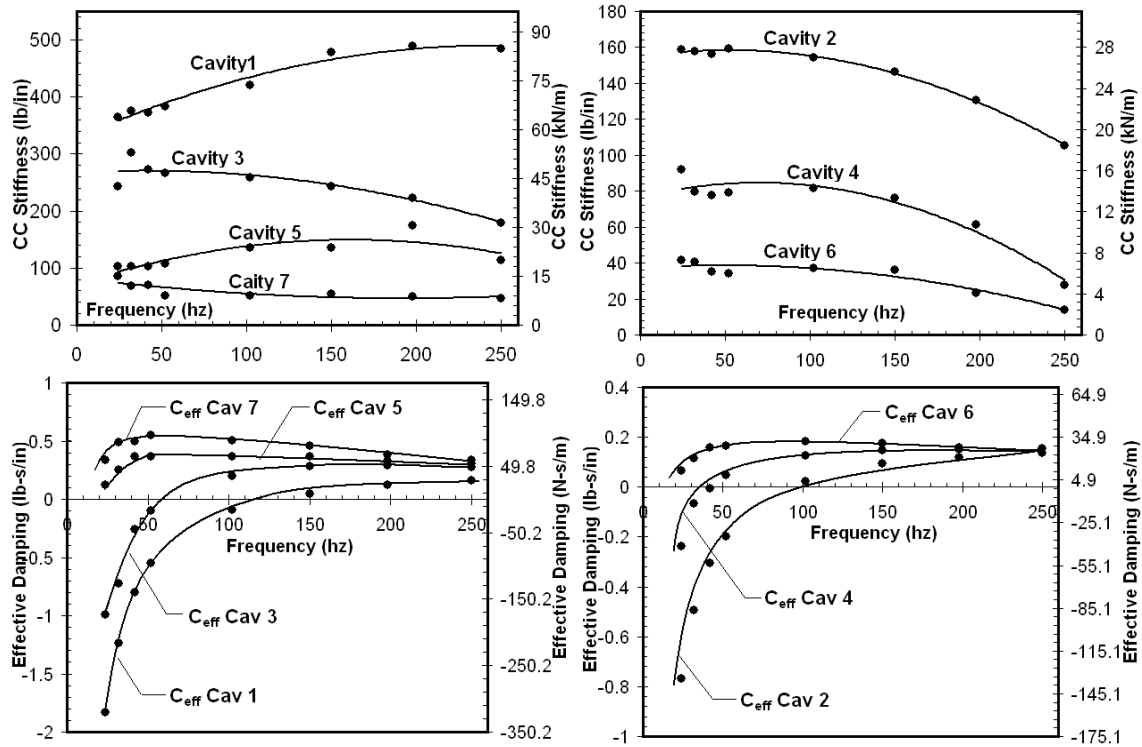


Figure 19. Cavity level rotordynamic coefficients: FPDS2 0RPM with preswirl

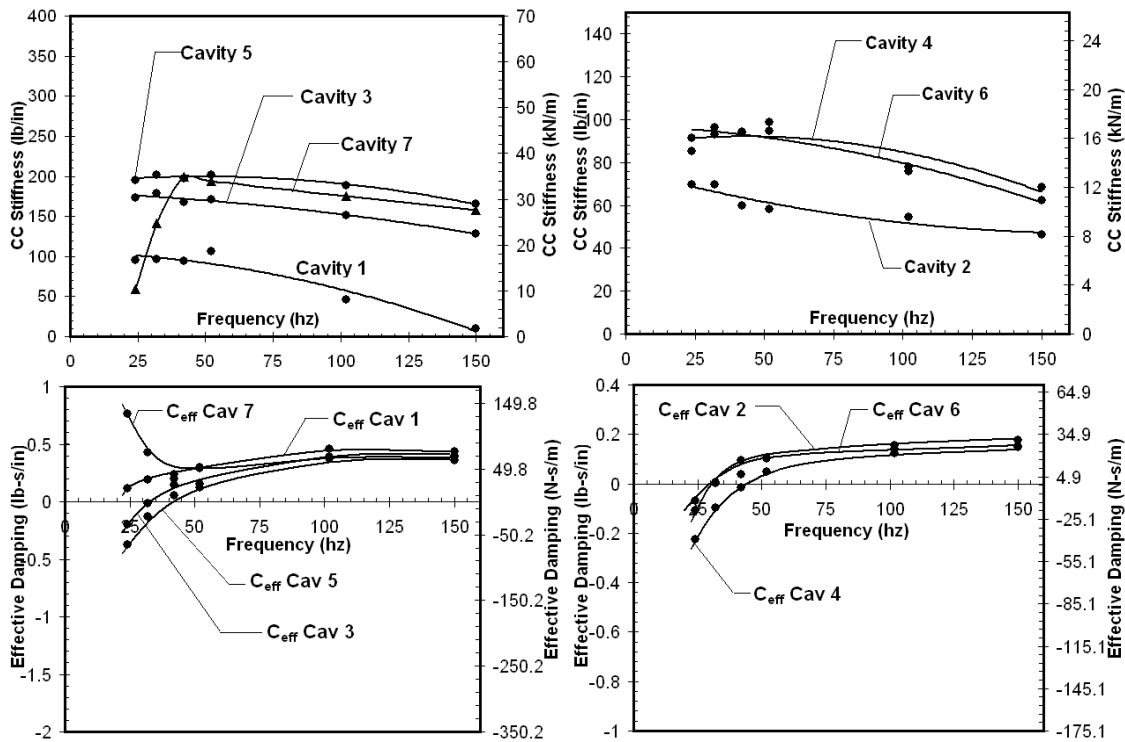


Figure 20. Cavity level rotordynamic coefficients: FPDS2 without preswirl 15krpm

The cross-coupled stiffness for this case is maximized in the center of the seal and drops in value towards the edge of the seal, whereas the effective damping is maximized at the seal end and portrays the higher crossover frequencies at the center. Plotting the crossover frequency results for the cases shown in Figs. 19-20, reveals the influence of rotor speed compared to preswirl on cavity crossover frequencies (Fig. 21). As mentioned earlier, the results indicate that preswirl has a stronger influence on effective damping than rotor speed, and presents high destabilizing effects at the upstream section of the seal that rapidly diminishes as the cavity number increases. Rotor speed on the other hand generates maximum destabilizing forces at the center of the seal, which decreases towards the ends of the seal.

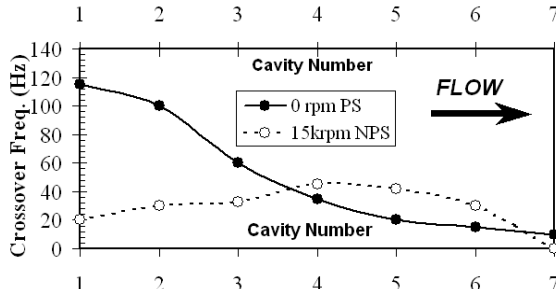


Figure 21. Cavity C_{eff} crossover frequencies: FPDS2

CONCLUSIONS

The rotordynamic performance of three annular gas seals was experimentally characterized in a controlled motion test rig. Results presented herein represent the first set of direct comparisons of rotordynamic force coefficients for these three types of seals under similar inlet preswirl conditions.

The seals' rotordynamic performance was evaluated in terms of effective damping and relevant crossover frequencies, which are functions of the cross-coupled stiffness and direct damping. The FPDS and HC seal revealed the largest destabilizing cross-coupled stiffness values that are strong functions of the inlet preswirl and rotor speed. On the other hand, the LABY seal portrayed a cross-coupled stiffness that seemed to have sensitivity only to inlet preswirl and not rotor speed. Interestingly enough, this behavior ultimately resulted in the LABY seal possessing superior stability characteristics at lower frequency ranges when considering conditions with no preswirl and high rotor speeds. Therefore, using a labyrinth seal in combination with a swirl break may be preferable seal configuration for rotors with a very low first mode natural frequency. However when considering inlet preswirl, the LABY seal showed to have negative effective damping for a large portion of the frequency range up to 100Hz. Under these preswirl conditions the FPDS and HC seal clearly outperformed the LABY seal by exhibiting lower cross over frequencies ranging from 40-60 Hz and generating an order of magnitude higher effective damping levels past the cross over frequency. Higher effective damping levels are reached despite the larger cross couple stiffness values due to the higher direct damping. In terms of the comparisons between the HC and FPDS, the damping coefficients were nearly insensitive to inlet preswirl and rotor speed for the HC seal, while in the case of the FPDS the values increased as the rotor speed increased and the preswirl increase (~20 %). This particular behavior proves to be the difference in terms of crossover frequency values between the FPDS and HC seal. Furthermore, experimental effective

damping results from Ref. [3] for a HC seal with a 0.75 L/D ratio (i.e. ~2 times larger than current test seal) subject to a high inlet pressure (70 bar) yielded similar crossover frequencies than those reported in the present study. The good correlation between the set of independent measurements may indicate that the current crossover frequency results could be extrapolated to more typical operating conditions found in centrifugal compressors. Currently, there is a test campaign on a new GE Oil and Gas test rig focused on verifying the results presented here using operating pressures representative of high-pressure centrifugal compressors.

The overall force coefficients identified from the pressure method yielded lower absolute values than the coefficient identified from impedance test, yet both results follow similar trends. Thus, the discrepancy in terms of the absolute values is attributed to the contribution to the seal reaction force of the dynamic pressure arising from the regions under the seal blades. Despite the observed discrepancies, both the pressure and impedance identification methods yielded identical crossover frequencies. The experimental results indicate that preswirl has a stronger influence on effective damping than rotor speed and that the destabilizing effects due to preswirl are higher at the beginning of the seal and rapidly diminish as the cavity number increases. Rotor speed, on the other hand, generates maximum destabilizing forces at the center of the seal, which decreases towards the ends of the seal.

The experimental findings from this study support the common approach of replacing traditional labyrinth seals with either "pocket" style or textured damper seals to improve the rotordynamic stability of process gas centrifugal compressors. This is especially true for inlet preswirl and when the first fundamental subsynchronous rotor mode is located above the cross over frequency of the seal's effective damping term. This is typically the case in most common centrifugal compressor applications where the rotor is supported on oil lubricated tilting pad bearings. On the other hand, in the case of softly mounted rotor bearing systems utilizing squeeze film dampers, the application of damper seals with negative effective damping at lower frequency ranges raises concern, which requires further research to improve the cross over frequency location for soft mounted rotor-bearing systems.

ACKNOWLEDGEMENTS

The authors would like to thank GE Oil and Gas and GE Global Research Center for allowing the publication of this work. The authors would like to also thank Dr. John Vance for helping with initial seal studies and Dr. Fouad Zeidan for supplying the FPDS.

NOMENCLATURE

A_{ij}	housing acceleration	$\text{kg} \cdot \text{m} / \text{s}^2$
C_{ij}	damping coefficient	$\text{N} \cdot \text{s} / \text{m}^2$
C_{EFF}	effective damping coefficient	$\text{N} \cdot \text{s} / \text{m}^2$
D_{ij}	relative housing displacement	m
F_{ij}	dynamic force on housing	N
\bar{F}	cavity pressure force	N
H_{ij}	mechanical impedance	N/m
K_{ij}	stiffness coefficient	N/m
m	housing mass	kg
P	peak dynamic cavity pressure	N / m^2
ω	excitation frequency of housing	Hz

ϕ_{ij} ,	pressure impedance	N/m
θ_o ,	angular location of cavity	deg

subscripts

i ,	direction of force or excitation
j ,	direction of response

superscripts

k ,	cavity number
-------	---------------

REFERENCES

[1] Childs, D. W., Vance, J. M., 1997, "Annular Gas Seals and Rotordynamics of Compressors and Turbines", *Proceedings of the Twenty Sixth Turbomachinery Symposium*, College Station, TX, pp. 201-220.

[2] Zeidan, F., Perez, R. X., Stephenson, M. E., 1993, "The use of Honeycomb Seals in Stabilizing Two Centrifugal Compressors", *Proceedings of the Twenty Second Turbomachinery Symposium*, College Station, TX, pp. 3-15.

[3] Sprowl, T. B., Childs, D., 2007, "A Study of the Effects of Inlet Preswirl on the Dynamic Coefficients of a Straight-Bore Honeycomb Gas Damper Seal," *ASME J. Eng. Gas Turbines Power.*, **129**(January), pp. 220-229.

[4] Vance, J. M., Zeidan, F., Murphy, B. T., *Machinery Vibrations and Rotordynamics*, 2010, pp. 91, John Wiley & Sons, New Jersey

[5] Dawson, M.P., Childs, D., 2002, "Measurements Versus Predictions for the Dynamic Impedance of Annular Gas Seals-Part II: Smooth and Honeycomb Geometries," *ASME J. Eng. Gas Turbines Power*, **124**(4), pp. 963-970.

[6] Smalley, A., Camatti, M., Childs, D., Hollingsworth, J., Vannini, G., Carter, J., 2006, "Dynamic Characteristics of the Diverging Taper Honeycomb-Stator Seal," *ASME J. Turbomach.*, **128**(4), pp. 717-724.

[7] Childs, D. W., Shin, Y., S., Seifert, B., 2008, "A Design to Improve the Effective Damping Characteristics of Hole Pattern Stator Annular Gas Seals", *ASME of Eng. Gas Turbines Power.*, **130**(1), 012505.

[8] Richards, R. L., Vance, J. M., Paquette, D. J., Zeidan, F., 1995, "Using a Damper Seal To Eliminate Subsynchronous Vibrations in Three Back-To-Back Compressors", *Proceedings of the Twenty Foruth Turbomachinery Symposium*, College Station, TX, pp. 59-71.

[9] Vance, J. M., and Shultz, R. R., 1993, "A New Damper Seal for Turbomachinery," *Proc. of the 14th Vibration and Noise Conference*, Albuquerque, NM, ASME DE 60, pp. 139-148.

[10] Alford, J.S., 1965, "Protecting Turbomachinery from Self Excited Rotor Whirl," *ASME J. Eng. Gas Turbine Power*, **87**(4), , pp. 333-344.

[11] Li, J., Kushner, F., and DeChoudhury, P., 2002, "Experimental Evaluation of Slotted Pocket Damper Seals on a Rotating Test Rig," *Proceedings of 47th ASME Turbo Expo Land Sea & Air conf.*, pp 230-240, June, Amsterdam, The Netherlands

[12] Ertas, B., Vance, J., 2007, "Rotordynamic Force Coefficients for a New Damper Seal Design," *ASME J. Tribol.*, **129**(April), pp. 365-374.

[13] Benckert , H. and Wachter, J., 1980, "Flow Induced Spring Coefficients of Labyrinth Seals for Application in Rotordynamics," NASA CP-21333, *Proceedings of the Workshop on Rotordynamic Instability Problems in High Performance Turbomachinery*, Texas A&M University, College Station, pp. 189-212.

[14] Childs, D., and Hale, K., 1994, "A Test Apparatus and facility to identify the Rotordynamic Coefficients of High-Speed Hydrostatic Bearings," *J. Tribol.*, **116**, pp. 337-334.

[15] Rouvas, C. and Childs, D., 1993, "A Parameter Identification Method for the Rotordynamic Coefficients of a High Reynolds Number Hydrostatic Bearing," *ASME J. Vib. Acoust.*, **115**(3), pp. 264-270.

[16] Ertas, B., Vance, J., Gamal, A., 2006, "Rotordynamic Force Coefficients of Pocket Damper Seals," *ASME J. Turbomach.*, **128**(4), pp. 725-737.

[17] Picardo, A., Childs, D., 2005, "Rotordynamic Coefficients for a Tooth-on-Stator Labyrinth Seal at 70 Bar Supply Pressures: Measurements Versus Theory and Comparisons to a Hole-Pattern Stator Seal," *ASME J. Eng. Gas Turbines Power*, **127**(4), pp. 843-855.